C. R. Mecanique 341 (2013) 152–160

Contents lists available at SciVerse ScienceDirect

Comptes Rendus Mecanique

www.sciencedirect.com

Combustion, flow and spray dynamics for aerospace propulsion

Numerical simulation of unsteady planar ammonium perchlorate flames including detailed gas phase chemistry and fluid–structure interaction

Simulation numérique instationnaire d'une flamme plane de perchlorate d'ammonium avec prise en compte d'une chimie détaillée en phase gazeuse et des interactions fluide–structure

Vincent Giovangigli [a,*], Shihab Rahman [b]

[a] *CMAP–CNRS, École polytechnique, 91128 Palaiseau cedex, France*
[b] *ONERA, chemin de la Huniere, BP 80100, 91123 Palaiseau cedex, France*

ARTICLE INFO

Article history:
Available online 11 January 2013

Keywords:
Flame
Propellant
Acoustics
Ammonium perchlorate
Complex chemistry

Mots-clés :
Flamme
Propergol
Acoustique
Perchlorate d'ammonium
Chimie complexe

ABSTRACT

A one-dimensional unsteady combustion model is presented for ammonium perchlorate flames taking into account a detailed gas phase chemistry with 36 species and 216 reactions, a fully-coupled fluid–structure interaction and allowing for acoustic and elastic waves propagation. The model is used to calculate a wave propagating from the gas phase into the solid phase and reflected by the interface. The interface temporal response shows a linear behavior for the test case of interest in this article.

RÉSUMÉ

Un modèle monodimensionnel de combustion instationnaire du perchlorate d'ammonium prenant en compte une chimie détaillée en phase gazeuse avec 36 espèces et 216 réactions, les interactions fluide–structure à l'interface et permettant la propagation d'ondes acoustiques et élastiques est présenté. Nous étudions la propagation d'une onde allant du gaz vers le solide et réfléchie par l'interface. La réponse temporelle de l'interface révèle un comportement linéaire pour le cas-test considéré dans ce travail.

1. Introduction

Unsteady combustion of solid propellants is an important source of instabilities in rocket motors [1]. The coupling between acoustics and combustion is of major interest and yet remains to be fully understood. Flame-acoustic interaction is often characterized by a transfer function linking the heat release rate fluctuations within the flame to the incident velocity perturbations [2,3]. For solid propellants, however, the quantity of interest is usually the pressure-coupled response function R_p defined as

$$R_p = \frac{m'/\overline{m}}{p'/\overline{p}} \tag{1}$$

* Corresponding author.
E-mail addresses: vincent.giovangigli@polytechnique.fr (V. Giovangigli), shihab.rahman@onera.fr (S. Rahman).

1631-0721/$ – see front matter
http://dx.doi.org/10.1016/j.crme.2012.10.017

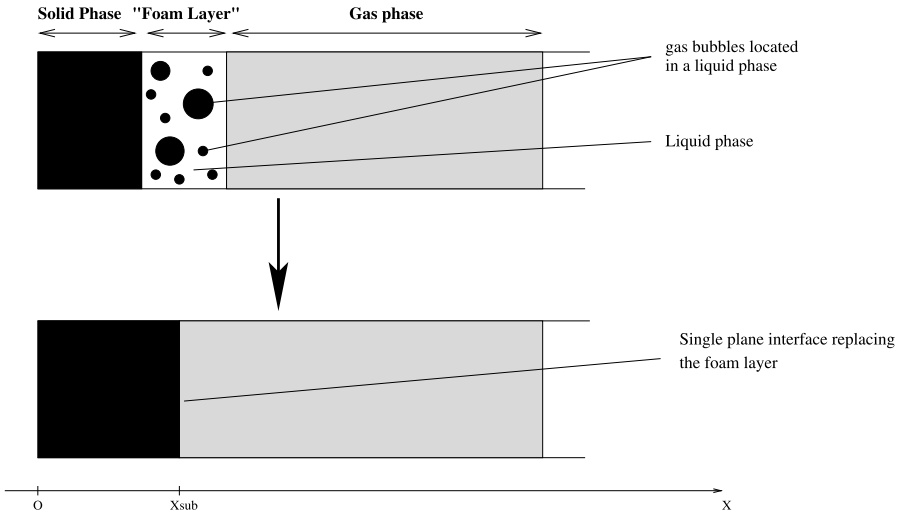

Fig. 1. One-dimensional model of AP with a lumped interface.

where $\overline{m}$ and $\overline{p}$ are respectively the steady-state mass flow rate and pressure at the propellant surface, and m' and p' are the corresponding unsteady fluctuations.

Over the past 60 years, the pressure-coupling phenomenon has mostly been theoretically addressed under the classical "Quasi-Steady Homogeneous One-Dimensional" or QSHOD assumptions [4–6]. Under these assumptions, small perturbations of the coupled gas–solid system are investigated through linearized equations. The gas phase may be investigated with the so-called Flame Model or FM theoretical framework [7], or by calculating steady-state sensitivity coefficients related to surface mass flow rate and surface temperature, which leads to the Zel'dovich–Novozhilov model or ZN [6,8].

The complex response function R_p obtained within the FM and ZN theoretical frameworks has been successful in showing the existence of one thermal peak resonance at moderate mean pressure and moderate gas phase pressure oscillation, occurring at the typical thermal frequency of the solid phase. Other works have established the necessity to release the quasi-steady gas phase assumption in order to draw a second resonant peak at higher oscillation frequencies [9]. From a numerical point of view, non-linear behavior has been found for sufficiently high gas phase pressure oscillations [10–12], though often using simplified chemical kinetics to describe the gas phase.

To improve existing models, the present work is concerned with a fully-coupled one-dimensional unsteady combustion model of Ammonium Perchlorate (AP) which is still a significant ingredient of propellants of practical use today. Such a model will provide new insight into the pressure-coupling phenomenon by taking into account a detailed gas phase chemistry, relaxing the quasi-steady and low Mach number assumptions in the gas phase, and allowing for thermal/mechanical coupling through the fluid–structure interaction at the propellant surface. Acoustic/elastic waves are introduced into the system by writing characteristic boundary conditions at the solid and gas phases external boundaries.

In Section 2, we present the equations of the model. In Section 3, we describe the numerical method. In Section 4, we present unsteady simulation results showing an acoustic/elastic wave propagating into the system and the interface response in term of the mass flow rate.

2. Theoretical model

2.1. A lumped interface model

A one-dimensional model of ammonium perchlorate (AP) requires the description of three regions: the solid phase, the gas phase and the intermediate "foam layer" as illustrated in Fig. 1. As experimental evidence [13] and numerical simulations [14] have established, the foam layer is generally of the order of magnitude of one micron in AP flames. The present model thus lumps the foam layer into an infinitely thin interface. Such an interface model has been validated with regards to steady combustion simulations [15] and unsteady linear ZN theory [16,17]. Taking into account a foam layer with nonzero thickness as well as more complex interface jump relations – as impedance conditions – are beyond the scope of this work.

Variables are defined in the laboratory frame of reference, that is, in the frame attached to the solid rocket motor (SRM). In order to avoid a dynamic meshing of the solid and gas phase domains, we use a coordinate system moving with the interface. Denoting by x^i the interface abscissa in the laboratory frame, x^{old} the space abscissa attached to the laboratory and x the space abscissa attached to the interface, we have $x = x^{old} - \int_0^t V^i_{lab}(\tau)\,\mathrm{d}\tau$, where t is the current time and $V^i_{lab} = \mathrm{d}x^i/\mathrm{d}t$ is the negative interface regression speed in the laboratory frame. Any unknown quantity $\varphi^{old}(t, x^{old})$ in the laboratory coordinate system is then rewritten $\varphi(t, x)$ in the new coordinate system.

2.2. Solid phase equations

No chemical reactions are taken into account in the solid phase in the absence of chemical data. The solid phase is assumed to undergo small deformations because of the high value of the Lamé coefficients and may be described with the linear thermo-elasticity theory [18]. Assuming no mean velocity in the solid phase and denoting the displacement by ξ, the deformation by ϵ and the solid phase velocity perturbation by u_{sl}, we have $\epsilon = \partial_x \xi$ and $u_{sl} = \partial_t \xi$.

2.2.1. Conservation equations in the solid phase

The solid mass conservation equation reads

$$\partial_t \rho_{sl} - V^i_{lab} \partial_x \rho_{sl} + \partial_x(\rho_{sl} u_{sl}) = 0 \tag{2}$$

where ρ_{sl} is the solid phase density and V^i_{lab} is the interface velocity in the laboratory frame of reference. The term $-V^i_{lab}\partial_x \rho_{sl}$ arises from the change of coordinate from the fixed system to the moving system. It is also established that $\rho_{sl0}/\rho_{sl} = \det(F)$, where ρ_{sl0} is the solid phase density in its initial configuration and F is the deformation gradient. Under the small deformation assumption, the mass conservation equation may also be written $\rho_{sl} = \rho_{sl0}$ at zeroth order. The momentum conservation equation reads

$$\partial_t(\rho_{sl} u_{sl}) - V^i_{lab}\partial_x(\rho_{sl} u_{sl}) + \partial_x\big(\rho_{sl} u^2_{sl} - \sigma_{sl}\big) = 0 \tag{3}$$

where σ_{sl} is the Cauchy tensor and linearizing this equation yields

$$\rho_{sl0}\big(\partial_t u_{sl} - V^i_{lab}\partial_x u_{sl}\big) - \partial_x \sigma_{sl} = 0 \tag{4}$$

Finally, total energy conservation can be written

$$\partial_t\left(\rho_{sl}\left(e_{sl} + \frac{1}{2}u^2_{sl}\right)\right) - V^i_{lab}\partial_x\left(\rho_{sl}\left(e_{sl} + \frac{1}{2}u^2_{sl}\right)\right) + \partial_x\left(\rho_{sl} u_{sl}\left(e_{sl} + \frac{1}{2}u^2_{sl}\right) + q_{sl} - \sigma_{sl} u_{sl}\right) = 0 \tag{5}$$

where e_{sl} is the internal energy and q_{sl} is the heat flux. Linearizing the energy conservation equation, denoting T_{sl} the solid phase temperature and c_{sl} the solid phase heat capacity, we obtain

$$\rho_{sl0} c_{sl}\big(\partial_t T_{sl} - V^i_{lab}\partial_x T_{sl}\big) + \partial_x q_{sl} = 0 \tag{6}$$

The elimination of the smaller convective term $\rho_{sl0} c_{sl} u_{sl} \partial_x T_{sl}$ uncouples the energy equations and simplifies the formulation of the NSCBC boundary conditions at the left external solid boundary. However, this term should be retained for future studies since it may influence the interface acoustic impedance. The kinematic compatibility relation between u_{sl} and ϵ_{sl} is finally

$$\partial_t \epsilon_{sl} - V^i_{lab}\partial_x \epsilon_{sl} = \partial_x u_{sl} \tag{7}$$

2.2.2. Expression of fluxes

Under the assumption of thermo-elastic behavior, σ_{sl} is given by

$$\sigma_{sl} = \kappa_{sl}\partial_x \xi + 2\mu_{sl}\partial_x \xi - (3\kappa_{sl} + 2\mu_{sl})\alpha_t (T - T_0) \tag{8}$$

where κ_{sl} and μ_{sl} are the Lamé coefficients of AP, α_t is the thermal dilatation coefficient, and T_0 is the initial temperature of AP. A further simplification consists in omitting the thermo-mechanical coupling in the latter equation, so that $\sigma_{sl} = \kappa_{sl}\partial_x \xi + 2\mu_{sl}\partial_x \xi$. Eqs. (4) and (7) then form a first order hyperbolic system, which is convenient for writing characteristic boundary conditions. Finally, denoting by λ_{sl} the solid thermal conductivity, the heat flux can be written $q_{sl} = -\lambda_{sl}\partial_x T_{sl}$.

2.3. Gas phase equations

2.3.1. Conservation equations

Total mass conservation is written as

$$\partial_t \rho_g - V^i_{lab}\partial_x \rho_g + \partial_x(\rho_g u_g) = 0 \tag{9}$$

where ρ_g is the gas density and u_g is the gas velocity. Species conservation is written as

$$\partial_t(\rho_g Y_k) - V^i_{lab}\partial_x(\rho_g Y_k) + \partial_x(\rho_g Y_k u_g + \mathcal{F}_k) = m_k \omega_k, \quad 1 \leqslant k \leqslant n \tag{10}$$

where Y_k is the mass fraction of the kth species, m_k is the molecular weight of the kth species, ω_k is the molar production rate of the kth species, $\mathcal{F}_k$ is the diffusion flux of the kth species, and n is the number of species. The gas phase momentum is conserved according to

$$\partial_t(\rho_g u_g) - V^i_{lab}\partial_x(\rho_g u_g) + \partial_x\big(\rho_g u_g^2 + p - \tau_g\big) = 0 \tag{11}$$

where τ_g is the viscous stress tensor and p is the gas pressure. Energy conservation is finally written

$$\rho_g c_p\big(\partial_t T_g - V^i_{lab}\partial_x T_g + u_g\partial_x T_g\big) + \partial_x\Big(q_g - \sum_{1\leqslant k\leqslant n} h_k\mathcal{F}_k\Big) = \partial_t p - V^i_{lab}\partial_x p + u_g\partial_x p + \tau_g\partial_x u_g - \sum_{1\leqslant k\leqslant n}\mathcal{F}_k c_{pk}\partial_x T_g - \sum_{1\leqslant k\leqslant n} h_k m_k\omega_k \tag{12}$$

where c_p is the mixture heat capacity at constant pressure, T_g is the gas temperature, q_g is the total heat flux, h_k is the enthalpy of the kth species, and c_{pk} is the heat capacity of the kth species at constant pressure.

2.3.2. Expression of transport fluxes

For a multi-component mixture in a one-dimensional flow, neglecting thermal diffusive and barodiffusive effects, the transport fluxes τ_g, $\mathcal{F}_k$, and q_g are given by [19]

$$\tau_g = \Big(\kappa + \frac{4}{3}\eta\Big)\partial_x u_g, \qquad \mathcal{F}_k = -\sum_{1\leqslant l\leqslant n} C_{kl}\partial_x X_l, \quad 1\leqslant k\leqslant n, \qquad q_g = -\lambda\partial_x T_g + \sum_{1\leqslant k\leqslant n} h_k\mathcal{F}_k \tag{13}$$

where κ is the bulk viscosity, η is the shear viscosity, C_{kl} is the multi-component flux diffusion coefficients, X_k is the mole fraction of the kth species, and λ is the thermal conductivity.

2.3.3. Gas phase chemistry

We consider a total number n_r of chemical reactions involving n species

$$\sum_{1\leqslant k\leqslant n}\nu^f_{ki}\chi_k \leftrightarrows \sum_{1\leqslant k\leqslant n}\nu^b_{ki}\chi_k, \quad 1\leqslant i\leqslant n_r \tag{14}$$

where χ_k is the chemical symbol for the kth species, and ν^f_{ki} and ν^b_{ki} are the forward and backward stoichiometric coefficients of the kth species in the ith chemical reaction. The chemical production rate ω_k for the kth species and the reaction rate of progress of the ith reaction τ_i then read

$$\omega_k = \sum_{1\leqslant i\leqslant n_r}\big(\nu^b_{ki} - \nu^f_{ki}\big)\tau_i, \qquad \tau_i = K^f_i\prod_{1\leqslant k\leqslant n}\Big(\frac{\rho_g Y_k}{m_k}\Big)^{\nu^f_{ki}} - K^b_i\prod_{1\leqslant k\leqslant n}\Big(\frac{\rho_g Y_k}{m_k}\Big)^{\nu^b_{ki}} \tag{15}$$

where K^f_i and K^b_i are the forward and backward reaction constants of the ith chemical reaction. The forward reaction constant K^f_i is usually evaluated with Arrhenius law $K^f_i(T_g) = A_i T_g^{b_i}\exp(-E_i/RT_g)$, where A_i is the pre-exponential factor, b_i is the pre-exponential exponent and E_i is the activation energy of the ith chemical reaction. The backward reaction constant is evaluated as $K^b_i(T_g) = K^f_i(T_g)/K^e_i(T_g)$ where K^e_i is the equilibrium constant of the ith reaction [19].

2.4. Interface

The lumped interface equations include the jump relations for conservation of mass, momentum, and energy, since the interface cannot store it, the continuity of temperature $T_{sl} = T_g$, and the interface chemical production rates. Total mass conservation across the interface reads

$$\rho^+_g\big(u^+_g - V^i_{lab}\big) = \rho^-_{sl}\big(u^-_{sl} - V^i_{lab}\big) \tag{16}$$

where the superscripts "+" and "−" respectively denote the gas and solid phases. Species conservation reads

$$\rho^+_g Y^+_k\big(u^+_g - V^i_{lab}\big) + \mathcal{F}^+_k = m_k\widehat{\omega}_k \tag{17}$$

where $\widehat{\omega}_k$ is the surface production rate of the kth species. Momentum is conserved across the interface according to

$$\rho^+_g u^+_g\big(u^+_g - V^i_{lab}\big) + \mathcal{P}^+_g = \rho^-_{sl}u^-_{sl}\big(u^-_{sl} - V^i_{lab}\big) - \sigma^-_{sl} \tag{18}$$

Finally, energy conservation across the interface can be written as

$$\rho^+_g\Big(e^+_g + \frac{u^{+2}_g}{2}\Big)\big(u^+_g - V^i_{lab}\big) + q^+_g + \big(p^+ - \tau^+_g\big)u^+_g = \rho^-_{sl}\Big(e^-_{sl} + \frac{u^{-2}_{sl}}{2}\Big)\big(u^-_{sl} - V^i_{lab}\big) + q^-_{sl} - \sigma^-_{sl}u^-_{sl} \tag{19}$$

and may also be rewritten in terms of enthalpies.

The interface AP decomposition mechanism has two reactions, following Guirao and Williams [20,15]

$$\mathrm{AP}(s) \to \mathrm{NH_3} + \mathrm{HClO_4}, \qquad \mathrm{AP}(s) \to \mathrm{AP}(l) \to \sum_{1\leqslant k\leqslant n} \widehat{\nu}_{k2}\chi_k$$

where $\sum_{1\leqslant k\leqslant n}\widehat{\nu}_{k2}\chi_k$ is a weakly reactive mixture typically taken to be an equilibrium mixture [15]. Letting $\widehat{\nu}_{k1}=1$ for $k\in\{\mathrm{NH_3},\mathrm{HClO_4}\}$ and $\widehat{\nu}_{k1}=0$ otherwise, the interface chemical production rate $\widehat{\omega}_k$ of the kth gaseous species, the interface destruction rate $\widehat{\omega}_{\mathrm{AP}}$ of AP, and the rate of progress of the two interface reactions $\widehat{\tau}_1$ and $\widehat{\tau}_2$ are then given by

$$\widehat{\omega}_k = \widehat{\nu}_{k1}\widehat{\tau}_1 + \widehat{\nu}_{k2}\widehat{\tau}_2, \qquad \widehat{\omega}_{\mathrm{AP}} = -\widehat{\tau}_1 - \widehat{\tau}_2, \qquad \widehat{\tau}_i = \widehat{A}_i \exp(-\widehat{E}_i/RT), \quad i=1,2 \tag{20}$$

where $\widehat{A}_i$ is the pre-exponential factor and $\widehat{E}_i$ is the activation energy of the ith interface reaction. From the conservation of mass, the mass flux at the interface is given by $m=\rho_{sl}(u_{sl}-V^i_{lab})=-W_{\mathrm{AP}}\widehat{\omega}_{\mathrm{AP}}$. In our application, we have used $\widehat{E}=\widehat{E}_1=\widehat{E}_2$ and $\widehat{A}=W_{\mathrm{AP}}(\widehat{A}_1+\widehat{A}_2)$ so that we recover the traditional pyrolysis law $m=\widehat{A}\exp(-\widehat{E}/RT)$. The species reaction rates $\widehat{\omega}_k$ may then be rewritten $\widehat{\omega}_k = m\widehat{Y}_k$ with

$$\widehat{Y}_k = \frac{W_k}{W_{\mathrm{AP}}}\frac{\widehat{\nu}_{k1}\widehat{A}_1\exp(-\widehat{E}_1/RT)+\widehat{\nu}_{k2}\widehat{A}_2\exp(-\widehat{E}_2/RT)}{\widehat{A}_1\exp(-\widehat{E}_1/RT)+\widehat{A}_2\exp(-\widehat{E}_2/RT)} = \frac{W_k}{W_{\mathrm{AP}}}\frac{\widehat{\nu}_{k1}\widehat{A}_1+\widehat{\nu}_{k2}\widehat{A}_2}{\widehat{A}_1+\widehat{A}_2}$$

keeping in mind that $\widehat{E}=\widehat{E}_1=\widehat{E}_2$ and $W_{\mathrm{AP}}=\sum_{1\leqslant k\leqslant n}\widehat{\nu}_{k1}W_k=\sum_{1\leqslant k\leqslant n}\widehat{\nu}_{k2}W_k$. Since the activation energies are equal, the interfacial rates correspond to the rates used in [15] and the reaction parameter α used in [15] has a natural kinetic interpretation. A difference with [15], however, is that the interface temperature $T=T_{sl}=T_g$ is now variable and determined by $m=\widehat{A}\exp(-\widehat{E}/RT)$. Finally, in the general situation where the surface reaction activation energies differ, the interface reaction relative mass fluxes $\widehat{Y}_k$, $1\leqslant k\leqslant n$, are then temperature dependent.

2.5. Boundary conditions

2.5.1. Gas phase

The right boundary conditions in the gas phase are written following the NSCBC method [21,22]. Characteristic decomposition of unsteady boundary equations reveal incoming and outgoing waves that can then be precisely controlled. In the present work, we neglect viscous and reactive terms to write the waves at the right gas phase boundary. In a coordinate system attached to the interface, the unsteady system of equations at the right boundary reads

$$\partial_t\rho_g - V^i_{lab}\partial_x\rho_g + \frac{1}{2\mathrm{c}_g^2}(\mathcal{L}_1+\mathcal{L}_3)+\frac{1}{\mathrm{c}_g^2}\mathcal{L}_2 = 0 \tag{21}$$

$$\partial_t T_g - V^i_{lab}\partial_x T_g + \frac{T_g}{\gamma p}\left(\frac{\gamma-1}{2}(\mathcal{L}_1+\mathcal{L}_3)-\mathcal{L}_2\right) - T_g\sum_{1\leqslant i\leqslant n}\frac{\overline{m}}{m_i}\mathcal{L}_{i+3} = 0 \tag{22}$$

$$\partial_t u_g - V^i_{lab}\partial_x u_g + \frac{1}{2\rho_g\mathrm{c}_g}(\mathcal{L}_3-\mathcal{L}_1) = 0 \tag{23}$$

$$\partial_t Y_k - V^i_{lab}\partial_x Y_k + \mathcal{L}_{3+k} = 0, \quad 1\leqslant k\leqslant n \tag{24}$$

where c_g is the gas phase acoustic velocity and $\mathcal{L}_i$ are wave variation amplitudes of incoming and outgoing waves [22]. Those are defined as linear combinations of the primitive variable gradients and we only present the expression of $\mathcal{L}_1$

$$\mathcal{L}_1 = (u_g-\mathrm{c}_g)\left(\partial_x p - \rho_g\mathrm{c}_g\partial_x u_g + p\sum_{i=1}^{n}\frac{\overline{m}}{m_i}\partial_x Y_i\right) \tag{25}$$

referring to [22] for more details. At the gas phase right boundary, the only incoming wave variation amplitude is $\mathcal{L}_1$. This wave carries on information from the outer domain into the computational domain and, unlike the other waves, it cannot be obtained from the computed solution [21,22]. To define the $\mathcal{L}_1$ wave at the gas phase boundary, we consider its definition in (25) and neglect the spatial dependence of the mixture molecular weight $\overline{m}$, dropping the term $p\sum_{i=1}^{n}\frac{\overline{m}}{m_i}\partial_x Y_i$. With a harmonic behavior for the pressure p, an expression for the velocity u_g can be obtained by using gas phase acoustic equations. The following expression for $\mathcal{L}_1$ is then obtained and can be used to enter an acoustic wave into the computational domain with a very good approximation

$$\mathcal{L}_1 = 2\mathrm{k}\big(u_g^e-\mathrm{c}_g^e\big)\Delta p\cos\left(\omega t + \mathrm{k}\int_0^t V^i_{lab}(\tau)\,\mathrm{d}\tau\right) \tag{26}$$

where k is the incoming wave number, Δp is the pressure wave amplitude, and u_g^e and c_g^e are respectively the gas velocity and acoustic velocity defined at the gas phase right boundary.

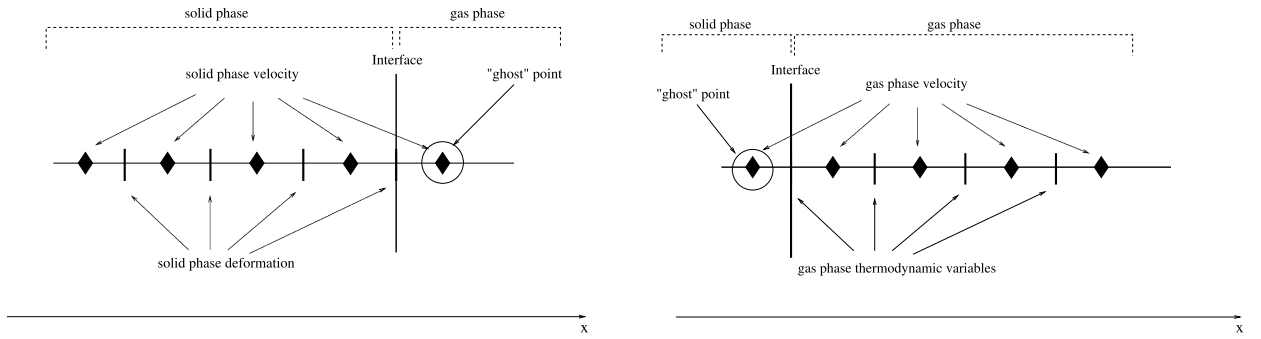

(a) Staggered grid in solid phase (b) Staggered grid in gas phase

Fig. 2. Staggered grid for computation domain.

2.5.2. Solid phase

The left solid phase boundary is also treated following the NSCBC method. Characteristic decomposition of solid phase equations yields the following system of equations

$$\partial_t \tilde{u}_{sl} - V^i_{lab}\partial_x \tilde{u}_{sl} + \mathsf{c}_{sl}(\mathcal{L}_{sl_1} - \mathcal{L}_{sl_2}) = 0 \tag{27}$$

$$\partial_t \epsilon - V^i_{lab}\partial_x \epsilon_{sl} + \mathcal{L}_{sl_1} + \mathcal{L}_{sl_2} = 0 \tag{28}$$

where c_{sl} is the solid phase acoustic velocity, and $\mathcal{L}_{sl_1}$ and $\mathcal{L}_{sl_2}$ are respectively solid phase incoming and outgoing wave variation amplitudes given by

$$\mathcal{L}_{sl_1} = \frac{1}{2}(-\partial_x \tilde{u}_{sl} + \mathsf{c}_{sl}\partial_x \epsilon_{sl}) \tag{29}$$

$$\mathcal{L}_{sl_2} = \frac{1}{2}(\partial_x \tilde{u}_{sl} - \mathsf{c}_{sl}\partial_x \epsilon_{sl}) \tag{30}$$

The present study is concerned with acoustic waves entering at the right gas phase boundary, propagating from gas phase to solid phase, and finally leaving the domain at the left solid phase boundary. Thus, at the solid phase boundary condition we must have

$$\mathcal{L}_{sl_1} = 0 \tag{31}$$

so that no acoustic wave can reenter the domain. Two additional wave propagation cases, however, are of practical interest. These are waves coming from gas phase and bouncing on a cramped solid boundary or waves entering from the solid phase boundary imposed by a vibrating engine. Though not treated in the present paper, those cases can be readily incorporated into the present formalism, modifying eventually the change of variable into the solid phase in order to take into account the cramped boundary in the coordinate system attached to the interface.

3. Numerical method

Spatial discretization of the governing equations has been performed with second order finite difference schemes on a "staggered" mesh as illustrated in Figs. 2(a) and 2(b). In the gas phase, velocity is defined at half-mesh points whereas thermodynamic variables are defined at integer mesh points. In the solid phase, the deformation variable is located at integer mesh points and the velocity at half-mesh points. These grids eliminate the usual checkerboard instabilities on pressure and deformation. In order to implement second order interface conditions and external boundary conditions, velocity ghost points have been introduced in the gas and solid phases. A second order Crank–Nicholson finite difference time discretization scheme has also been used.

A spatial second order scheme has been chosen in order to maintain a block tridiagonal structure of the Jacobian matrix, easing Newton's method with a fully implicit algorithm [23]. The attenuation of the pressure waves has been found sufficiently weak and the characteristic boundary conditions have been tested to allow the elimination of outgoing waves in the solid and gas phases [24]. Several test cases regarding scaling factor values and Newton's residuals were undergone in order to find the best compromise between precision and CPU time, and Newton's method tolerance was typically 10^{-5}. The solid phase domain extends from the left boundary $x = 0$ cm to the interface located at $x = 10$ cm and the gas phase from $x = 10$ cm up to the gas right boundary $x = 110$ cm and we have typically used 10 000 non-equispaced grid points.

The discretized equations are assembled in a single system and solved in a fully-coupled and implicit manner combining an explicit Euler predictor scheme and an implicit Newton's corrector method. This is the *monolithic* approach already used in nonreactive flows [25]. It has also been used in small Mach number models of propellants [26,27] as well as spray diffusion flames [28]. In the gas phase, highly vectorized CHEMKIN II subroutines [29,30] provide the calculated thermochemistry properties and the EGLIB software provides optimized calculation of the multi-component transport coefficients [31–34].

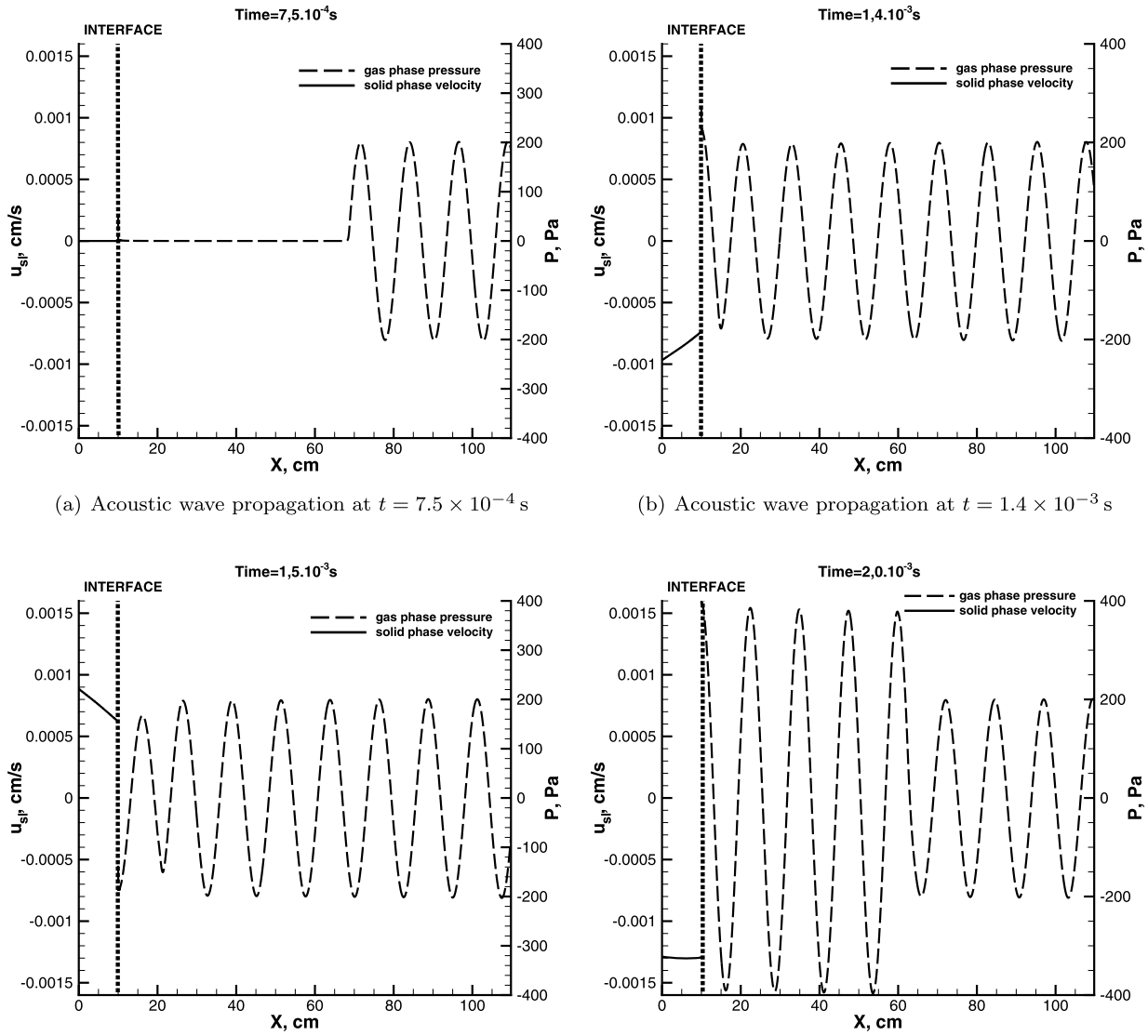

(a) Acoustic wave propagation at $t = 7.5 \times 10^{-4}$ s

(b) Acoustic wave propagation at $t = 1.4 \times 10^{-3}$ s

(c) Acoustic wave propagation at $t = 1.5 \times 10^{-3}$ s

(d) Acoustic wave propagation at $t = 2.0 \times 10^{-3}$ s

Fig. 3. An acoustic wave propagating from gas phase to solid phase.

4. Results

4.1. Flame parameters

The gas phase chemistry consists in $n = 36$ species reacting through $n_r = 216$ reactions [15]. A low value of pyrolysis law activation energy $\widehat{E} = 8$ kcal/mol has been used with and relatively high value of propellant initial temperature, 400 K, in order to avoid potential intrinsic instability issues [16]. The pyrolysis law pre-exponential factor $\widehat{A}$ has been selected to obtain a surface temperature of 825 K for a burning velocity of 0.3 cm/s, that is, at gas phase pressure of 20 atm and propellant initial temperature of 300 K. The end pressure p_g^e is fixed at a value of 216 bar and the steady regression rate of the interface is then $V_{lab}^i = -1.5$ cm/s.

4.2. Wave propagation from gas phase to solid phase

Fig. 3 shows a typical unsteady calculation, representing gas phase overpressure/underpressure in dashed line at the right-hand side of the interface and solid phase velocity in solid line at the left-hand side. Due to the slow kinetics of nitrogen-based components, a relatively large gas phase domain is required in order to reach chemical equilibrium and justify the dropping of reactive and viscous terms in the boundary conditions.

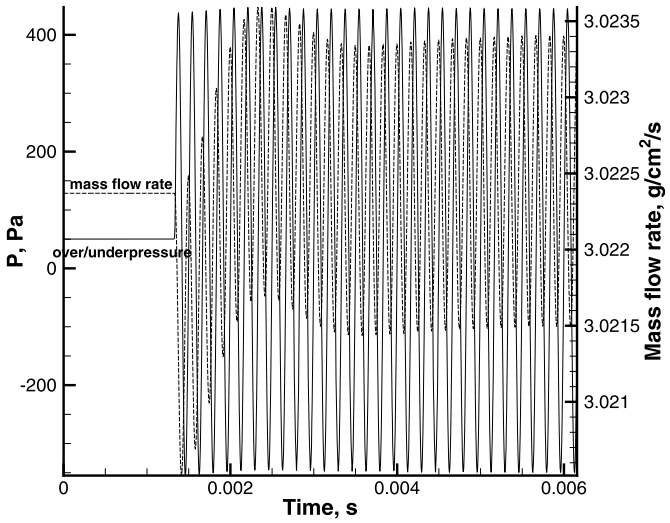

Fig. 4. Interface temporal response: interface overpressure and mass flow rate as functions of time.

The acoustic wave is initially introduced from the gas phase boundary with an amplitude of 200 Pa. It propagates with negligible attenuation and reaches the interface, where the solid is put to motion as suggested by the plotting of solid phase velocity in Fig. 3. It can be seen that an overpressure leads to negative solid phase velocity since it pushes the interface leftward, whereas an underpressure pumps up the solid towards the gas phase leading to positive solid phase velocity. The second thing to notice is the difference in solid phase and gas phase acoustic wave lengths. A typical gas phase acoustic velocity is indeed 700 m/*s*, whereas in the crystal AP it is 15 km/s. After the incoming of the gas phase acoustic wave toward the interface, the latter reflects a wave at exactly the same frequency as the incoming wave. This process is not disturbed by the action of solid phase since waves propagate into the solid phase without being reflected at solid boundary. Combination of incident and reflected waves that have similar frequencies finally lead to a stationary wave progressively reaching back the gas phase boundary.

4.3. Interface temporal response

Fig. 4 shows a typical interface temporal response. The overpressure/underpressure at interface is represented in solid line, and mass flow rate at interface is represented in dotted line as functions of time. The steady behavior first observed corresponds to the time required by the gas phase acoustic wave to reach the interface. Then, an overall harmonic mass flow rate response is obtained to a harmonic pressure solicitation, though the mean mass flow rate needs a transitory time to stabilize. A linear behavior similar to that observed in other studies [10,11] is thus obtained for this test case where acoustic waves propagate into the solid phase without bouncing off the solid boundary. It should be noted that, in the linear regime, the interface response over a wide frequency range can be investigated with a single calculation by introducing an input wave consisting in a linear “frequency sweep” [35], or containing the sum of several frequencies.

5. Conclusion

A one-dimensional unsteady combustion model has been developed for ammonium perchlorate that takes into account a detailed gas phase chemistry, fully-coupled fluid–structure interaction and allows for acoustic/elastic waves propagation. The model has been used to calculate an acoustic/elastic wave propagating from gas phase into solid phase and reflected by the interface. It is shown in particular that the interface reflects back a wave of the same frequency as the incident wave and the interface temporal response shows a linear behavior for the test case considered.

Other test cases of practical interest could further be simulated as waves bouncing off at a cramped solid boundary or waves generated from this boundary by the engine. These responses could then be spectrally analyzed and further lead to a response function to be compared with that of classical linear theories, like Zel’dovich–Novozhilov theory [24].

References

[1] F.E.C. Culick, Unsteady Motions in Combustion Chambers for Propulsion Systems, AGARDograph AG-AVT-039, RTO/NATO, Neuilly sur Seine, France, 2006.
[2] D. Durox, T. Schuller, S. Candel, Combustion dynamics of inverted conical flames, Proceedings of the Combustion Institute 30 (2005) 1717–1724.
[3] F. Boudy, D. Durox, T. Schuller, S. Candel, Nonlinear mode triggering in a multiple flame combustor, Proceedings of the Combustion Institute 33 (2011) 1121–1128.

[4] F.E.C. Culick, A review of calculations for unsteady burning of a solid propellant, AIAA Journal 6 (1968) 2241–2255.
[5] R.W. Hart, F.T. McClure, Combustion instability: Acoustic interaction with a burning propellant surface, The Journal of Chemical Physics 30 (1959) 1501–1514.
[6] B.V. Novozhilov, Burning of a powder under harmonically varying pressure, Journal of Applied Mechanics and Technical Physics 6 (1965) 141–144.
[7] L. De Luca, Theory of nonsteady burning and combustion stability of solid propellants by flame models, in: Progress in Astronautics and Aeronautics, vol. 143, 1991.
[8] Y.B. Zel'dovich, On the theory of combustion of powders and explosives, Journal of Experimental and Theoretical Physics 12 (1942) 498–524.
[9] J.S. T'ien, Oscillatory burning of solid propellant including gas phase time lag, Combustion Science and Technology 5 (1972) 47–54.
[10] K.R.A. Kumar, Computational studies on certain problems of combustion instability in solid propellants, PhD thesis, Indian Institute of Science, Bangalore, 2001.
[11] B. Rasmussen, R.A. Frederick Jr., Nonlinear heterogeneous model of composite solid-propellant combustion, Journal of Propulsion and Power 18 (2002) 1086–1092.
[12] M. Ali Ak, H. Vural, A time-operator splitting method for numerical analysis of 1-D solid propellant non-linear combustion response, in: 39th AIAA/ASME/SAE/ASEE Joint Propulsion Conference and Exhibit, Huntsville, Alabama, 20–23 July 2003.
[13] T.L. Boggs, Deflagration rate, surface structure, and subsurface profile of self-deflagrating single crystals of ammonium perchlorate, AIAA Journal 8 (1970) 867–872.
[14] M. Tanaka, M.W. Beckstead, A three phase combustion model of ammonium perchlorate, AIAA Paper 96-2888, 1–3 July 1996.
[15] V. Giovangigli, N. Meynet, M. Smooke, Application of continuation techniques to ammonium perchlorate plane flames, Combustion Theory and Modelling 10 (2006) 771–798.
[16] S. Rahman, V. Giovangigli, V. Borie, Pressure and initial temperature sensitivity coefficient calculations in ammonium perchlorate flames, Journal of Propulsion and Power 27 (2011) 1054–1063.
[17] S.B. Margolis, R.C. Armstrong, Two asymptotic models for solid propellant combustion, Combustion Science and Technology 47 (1986) 1–38.
[18] J.D. Achenbach, Wave Propagation in Elastic Solids, North-Holland Publishing Company, 1973.
[19] V. Giovangigli, Multicomponent Flow Modeling, Birkhauser Boston, 1999.
[20] C. Guirao, F.A. Williams, A model for ammonium perchlorate deflagration between 20 and 100 atm, AIAA Journal 9 (1971) 1345–1356.
[21] M. Baum, T. Poinsot, D. Thévenin, Accurate boundary conditions for multicomponent reactive flows, Journal of Computational Physics 116 (1994) 247–261.
[22] T.J. Poinsot, D. Veynante, Theoretical and Numerical Combustion, second edition, R.T. Edwards, 2005.
[23] M.D. Smooke, J.A. Miller, R.J. Kee, Determination of adiabatic flame speeds by boundary value methods, Combustion Science and Technology 34 (1983) 79–89.
[24] S. Rahman, Modélisation et simulation numérique de flammes planes instationnaires de perchlorate d'ammonium, PhD thesis, Université Paris 6, 2012.
[25] E. Walhorn, A. Kölke, B. Hübner, D. Dinkler, Fluid structure coupling within a monolithic model involving free surface flows, Computers and Structure 83 (2005) 2100–2111.
[26] K. Prasad, R. Yetter, M.D. Smooke, An eigenvalue method for predicting the burning rates of RDX propellants, Combustion Science and Technology 124 (1997) 35–82.
[27] K. Prasad, R. Yetter, M.D. Smooke, An eigenvalue method for predicting the burning rates of HMX propellants, Combustion and Flame 115 (1998) 406–416.
[28] R. Bendakhlia, V. Giovangigli, D. Rosner, Soret effects in laminar counterflow spray diffusion flames, Combustion Theory and Modelling 6 (2002) 1–17.
[29] R.J. Kee, F.M. Rupley, J.A. Miller, Chemkin II: A Fortran chemical kinetics package for the analysis of gas phase chemical kinetics, Technical Report SAND89-8009B, SANDIA National Laboratories, 1989.
[30] V. Giovangigli, N. Darabiha, Vector computers and complex chemistry combustion, in: Mathematical Modeling in Combustion and Related Topics, Martinus Nijhoff Publishers, 1988, pp. 491–503.
[31] A. Ern, V. Giovangigli, Fast and accurate multicomponent transport property evaluation, Journal of Computational Physics 120 (1995) 105–116.
[32] A. Ern, V. Giovangigli, The structure of transport linear systems in dilute isotropic gas mixtures, Physical Review E 53 (1996) 485–492.
[33] A. Ern, V. Giovangigli, Optimized transport algorithms for flame codes, Combustion Science and Technology 118 (1996) 1989–1996.
[34] A. Ern, V. Giovangigli, EGLIB, a multicomponent transport software for fast and accurate evaluation algorithms, http://www.cmap.polytechnique.fr/www.eglib/home.html.
[35] F. Richecoeur, S. Ducruix, P. Scouflaire, S. Candel, Effect of temperature fluctuations on high frequency acoustic coupling, Proceedings of the Combustion Institute 32 (2009) 1663–1670.